ELSEVIER

Journal of Power Sources 104 (2002) 101–107

JOURNAL OF POWER SOURCES

www.elsevier.com/locate/jpowsour

Improving the high-temperature performance of $LiMn_2O_4$ spinel by micro-emulsion coating of $LiCoO_2$

Zhaolin Liu[a,*], Hongbin Wang[a], Ling Fang[a], Jim Y. Lee[a,b], Leong Ming Gan[a]

[a]*Institute of Materials Research and Engineering, 3 Research Link, Singapore 117602, Singapore*
[b]*Department of Chemical and Environmental Engineering, National University of Singapore, Singapore 119260, Singapore*

Received 21 May 2001; accepted 6 August 2001

Abstract

$LiMn_2O_4$ spinel, which has known performance deficiency in rechargeable lithium batteries at elevated temperatures, is coated with grains of $LiCoO_2$ through a novel micro-emulsion process. The resulting composite is characterized by elemental analysis, thermogravimetric analysis, differential scanning calorimetry, powder X-ray diffraction (XRD), and scanning and transmission electron microscopies. For assessment of electrochemical performance, the coated spinel is charged and discharged under typical conditions of battery application, and its cycleability and storage characteristics are determined at 55 °C. The results show substantially improved high-temperature performance, with a small reduction in capacity and specific energy relative to the pristine spinel.

Keywords: $LiMn_2O_4$; Micro-emulsion coating; Rechargeable lithium battery; Cycleability; High-temperature

1. Introduction

The demand for rechargeable batteries with high specific energies for portable electronic products has propelled lithium-based systems to market dominance. Lithium cobalt oxide, with its excellent application performance, is currently the standard cathode material in commercial lithium-ion batteries. There is concern, however, that the cost of cobalt may eventually limit the market growth of the lithium-ion batteries.

As the cost of manganese is about five times lower than that of cobalt, lithium manganese oxide spinel, $LiMn_2O_4$, is an attractive alternative. It is also more environmentally compatible and safer to handle. By contrast, the cycleability of $LiMn_2O_4$ leaves much to be desired, particularly at elevated temperatures. Investigations have shown that the capacity fading upon cycling or with storage at high temperatures is primarily the result of spinel dissolution in the electrolyte [1–4]. Tarascon and coworkers [5] have reported that the capacity loss during storage at elevated temperatures is a function of the surface area of the oxide. For a spinel electrode in the charged state, the failure begins at the spinel/electrolyte interface due to slow oxidation of the electrolyte at the high open-circuit potential of the cathode. This reaction is accelerated at high temperatures and produces deleterious by-products. For a spinel in the discharged state, HF-induced manganese dissolution is the major failure mechanism at high temperatures [5,6]. Tarascon and coworkers [5,6] also showed that the storage properties of $LiMn_2O_4$-based spinels at elevated temperatures could be improved by surface treatment. Basically, they coated $LiMn_2O_4$ with lithium boron oxide (LBO) glasses and also applied complexing acetylacetone as a surface treatment. Some encouraging results were obtained.

A similar approach to that of Tarascon and coworkers [5,6] is used here, but with $LiCoO_2$ as the coating material. A uniform coating of $LiCoO_2$ is applied to a spinel surface to reduce the contact between the spinel and the electrolyte, and thereby reduce the propensity of spinel dissolution in the electrolyte. The $LiCoO_2$ coating is deposited by a micro-emulsion-based process which enhances the uniformity of the surface coverage.

A micro-emulsion is generally defined as a system composed of a mixture of water or brine, hydrocarbon(s) and amphiphilic compound(s) in the form of a thermodynamically stable and optically isotropic solution [7]. The term 'amphiohiles' refers to surfactants as well as co-surfactants, such as a short chain alcohols. A transparent micro-emulsion can be formed as droplets of oil-swollen micelles dispersed in water (known as an oil-in-water (o/w) micro-emulsion), or water-swollen micelles dispersed in oil (known as a

* Corresponding author. Tel.: +65-874-8111; fax: +65-872-0785.
E-mail address: zl-liu@imre.org.sg (Z. Liu).

0378-7753/02/$ – see front matter
PII: S0378-7753(01)00878-3

water-in-oil (w/o) micro-emulsion). In between o/w and w/o micro-emulsion regions, there may exist bicontinuous micro-emulsions, where oil and water domains are randomly interconnected to form sponge-like nanostructures. In this aspect, inverse and bicontinuous micro-emulsions may be ideal media for the preparation of nanosize particles. This is because the numerous water domains in a micro-emulsion can serve as 'microreactors' for controlling the particle size. Nanoparticles of metals [8–11], metal oxides [12], metal carbonates [13,14], semiconductors, such as CdS [15], silver halides [16], Mn-doped ZnS nanocrystallites [17], Ru–Cu oxide/silica catalysts [18], La–Ni oxalates [19], La–Cu oxalates and Ba–Pb oxalates [20] have been successfully prepared by the micro-emulsion technique. These oxalate mixtures could readily be converted to the corresponding pervoskite-type mixed metal oxides by calcination.

2. Experimental

The micro-emulsion phase diagram used in this study is shown in Fig. 1. The micro-emulsion consisted of cyclohexane as the oil, NP9 as the nonionic surfactant of poly-(oxyethylene)$_9$ phenol ether, and aqueous solutions of various concentrations of 1 M $LiNO_3$ and 1 M $Co(NO_3)_2$. This micro-emulsion phase diagram was obtained by filtrating the aqueous salt solution to a given amount of cyclohexane-NP9 mixture in a screw-capped tube at room temperature to establish the clear turbid boundary. The shaded area enclosed by the boundary is the transparent micro-emulsion region.

Thermogravimetric analysis (TGA) and differential scanning calorimetry (DSC) characterizations of the coated $LiMn_2O_4$ spinel in air were carried out on a SDT2960 unit from TA Instruments. The temperature was scanned from 40 to 900 °C at 10 °C min^{-1}. The cobalt content in the composite was determined by inductively coupled plasma (ICP) spectroscopy using digestions of the composites in a mixture of 1 M HCl and 1 M HNO_3. Powder X-ray diffractometry was conducted on a Philips PW1877 diffractometer using Cu Kα radiation and a graphite monochromator. A Hitachi S4100 scanning electron microscope fitted with a Philips PV9900 energy dispersive analyzer provided morphological examination and point-to-point elemental analysis of the sample. Selected powder samples were also examined by high-resolution transmission electron microscopy on a Philips CM300 field emission microscope. Sample preparation in this case involved the ultrasonic dispersion of the powder in ethanol; the sample suspension was dispensed on standard copper TEM grids followed by carbon coating.

For half-cell studies, the $LiMn_2O_4$ and coated $LiMn_2O_4$ powder were mixed with 10 wt.% carbon black and 10 wt.% PVDF in 1-methyl-2-pyrrolidone (NMP). The slurry was used to coat 20-μm thick Al disks of 16 mm diameter to a mass loading of 40–50 mg cm^{-2} after drying (at 120 °C) and compaction (at 2.0 MPa). Each coated electrode was assembled into a 2016 coin cell using a Li counter electrode, a microporous polypropylene separator, and an electrolyte of 1 M $LiPF_6$ in a 50:50 (w/w) mixture of ethylene carbonate (EC) and diethyl carbonate (DEC). Cell assembly was carried out in an Ar-filled glove box with <1 ppm each of oxygen and moisture. The cells were charged and discharged at 25 °C using a Bitrode life cycle tester. All the cells were charged to 4.4 V and discharged to 3.3 V using a constant current density of 0.5 mA cm^{-2}. For tests of spinel dissolution, a beaker-type three-electrode cell (in an Ar-filled glove box) was used; Li foil was used for both the anode and the reference electrodes. The electrolyte solution was sampled intermittently during the cycling test and analyzed by ICP.

3. Results and discussion

3.1. Synthesis and characterization

The key objective of surface coating is to form a uniform protective layer. A number of solution-based techniques may be used, such as sol–gel transformation, solution

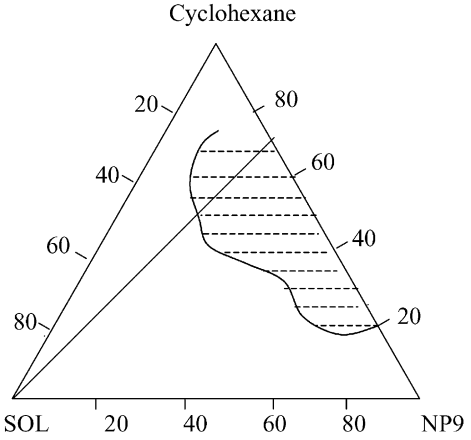

Fig. 1. Phase diagram for system consisting of cyclohexane-(NP9)-aqueous solutions of 0.1 M $LiNO_3$/0.1 M $Co(NO_3)_2$ at room temperature.

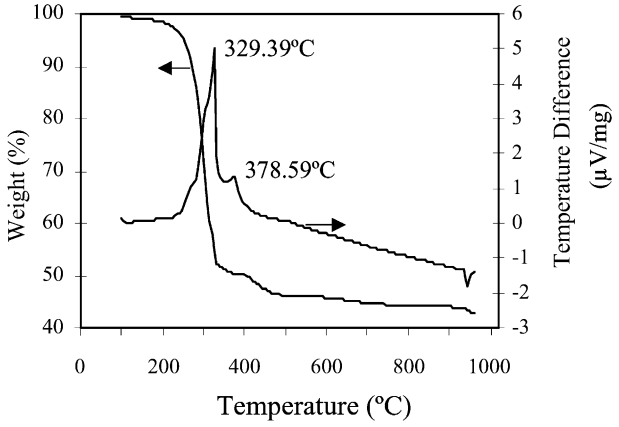

Fig. 2. TG–DTA curves for $LiCoO_2$-coated spinel from the emulsion drying method at 200 °C

precipitation, and micro-emulsion. The micro-emulsion composition at point P in the phase diagram of Fig. 1 was used together with $LiMn_2O_4$ powder for the subsequent preparation of $LiCoO_2$-coated $LiMn_2O_4$. This was achieved by adding a stoichiometric amount of the micro-emulsion P to spinel $LiMn_2O_4$ powder with stirring for about 12 h at 35 °C. The mixture was first dried at 110 °C before and then calcined in oxygen using a ramp rate of 5 °C min^{-1} to 756 °C for a total of 10 h. The calcined product ($LiCoO_2$-coated $LiMn_2O_4$) was cooled to room temperature at 1 °C min^{-1}. Different amounts of $LiMn_2O_4$ spinel were mixed with micro-emulsion P to obtain 1–11 wt.% $LiCoO_2$ in the composites. The TG–DTA curves of the as-deposited powder obtained by drying the micro-emulsion mixture at 200 °C for 1 h are shown in Fig. 2. The measurements were performed at a rate of 10 °C min^{-1} in air. Weight loss and two exothermic peaks were detected in the temperature range from 300 to 400 °C. These are mainly caused by the evaporation of the residual solvent and the combustion of organic compounds such as poly(oxyethylene)$_9$ phenol ether (NP9). The advantage of using a micro-emulsion technique is the attainment of a more uniform surface coating of $LiCoO_2$ on $LiMn_2O_4$

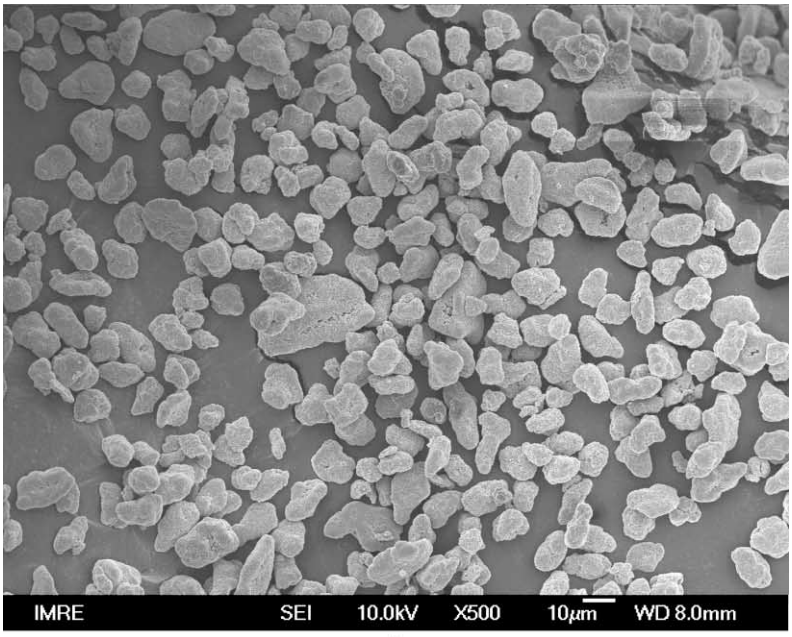

(a)

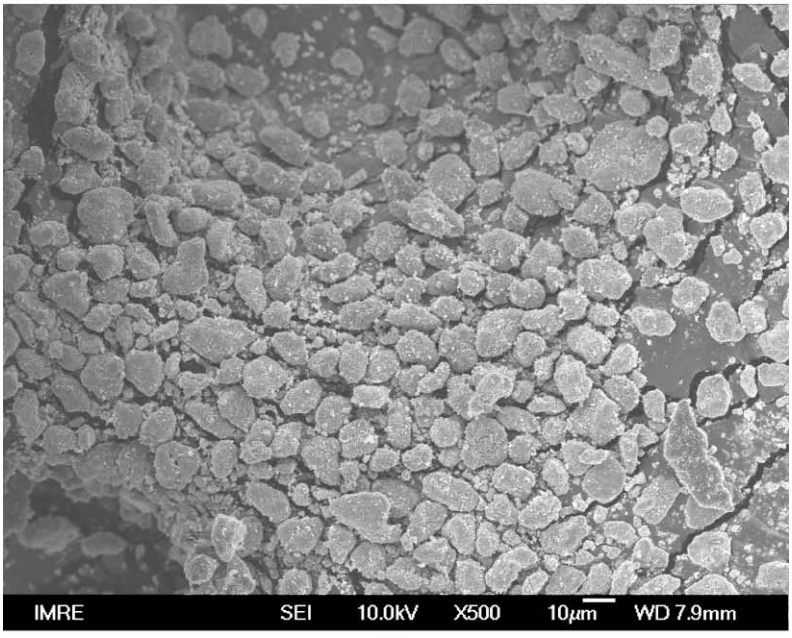

(b)

Fig. 3. Scanning electron micrographs of $LiMn_2O_4$ powder: (a) before and (b) after 5 wt.% $LiCoO_2$ surface treatment.

particles before and after calcination. Before calcination, the dispersed $LiMn_2O_4$ particles were stabilized by the surfactant NP9. Due to the presence of NP9 on the particle surface, the sintering of particles during the calcination is minimized.

$LiCoO_2$ grains were found on the surface of $LiMn_2O_4$ particles in all of the composite samples. From powder X-ray diffraction (XRD), the diffraction peaks of $LiCoO_2$/$LiMn_2O_4$ composite particles with <4 wt.% $LiCoO_2$ were characteristic of the spinel structure of $LiMn_2O_4$ with a cubic lattice parameter of 8.24 Å. The $LiCoO_2$ phase in the composite was too low to be detected by XRD at this level. The addition of more than 4 wt.% $LiCoO_2$ results in mixed phases of $LiMn_2O_4$ and $LiCoO_2$. In addition to the diffractions from $LiMn_2O_4$ spinel, there were other peaks that can be indexed by a hexagonal lattice of the α-$NaFeO_2$ (*R3m*) type [21].

The surface morphology of standard and surface-treated $LiMn_2O_4$ as examined by scanning electron microscopy is shown in Fig. 3. The surface of $LiMn_2O_4$ after treatment was decorated with small $LiCoO_2$ particles of 1-μm diameter or less, and loses the smooth contour originally present in untreated $LiMn_2O_4$ (Fig. 3b). The number of such 'foreign' particles increases with the amounts of lithium and cobalt nitrates used during the micro-emulsion preparation. When the $LiCoO_2$ content higher than 6 wt.%, some isolated particles of $LiCoO_2$ are also detected, along with $LiCoO_2$-coated $LiMn_2O_4$. Closer examination of the particle surface by HRTEM finds the presence of a 5-nm thick $LiCoO_2$ layer (light area in Fig. 4) on most of the spinel surface (dark area in Fig. 4). It is believed that most of the $LiMn_2O_4$ surface is protected by thin layers of $LiCoO_2$, with excess of $LiCoO_2$ salting out as a separate phase to decorate the spinel phase. The coating therefore decreases the direct contact of spinel particles with the electrolyte and is expected to reduce the capacity fading through particle dissolution in the electrolyte.

3.2. Electrochemical properties

The electrochemical performance of pristine and $LiCoO_2$ encapsulated spinel was examined in Li half-cells. Typical charge and discharge curves of encapsulated spinel with 5 wt.% $LiCoO_2$ at a current density of 0.2 mA cm^{-2} at 25 °C are presented in Fig. 5. The Li/$LiMn_2O_4$ cell had an initial charge capacity of 140 mAh g^{-1}, which is close to the theoretical value (148 mAh g^{-1}). This shows that about 0.94 mol Li^+ can be extracted from the spinel, to give a final composition of $Li_{0.06}Mn_2O_4$. The electrode delivered a reversible capacity of 139 mAh g^{-1} upon discharge with a two-step voltage profile. The 5 wt.% $LiCoO_2$-coated $LiMn_2O_4$ behaved similarly, as far as the shape of the charge and discharge profile is concerned. The first discharge capacity and the BET surface of $LiCoO_2$/$LiMn_2O_4$ composites (1, 3, 5, 7, 9 and 11 wt.% $LiCoO_2$) as a function of the $LiCoO_2$ content are given in Fig. 6. There is some slight decrease in the capacity (to 123 mAh g^{-1}) relative

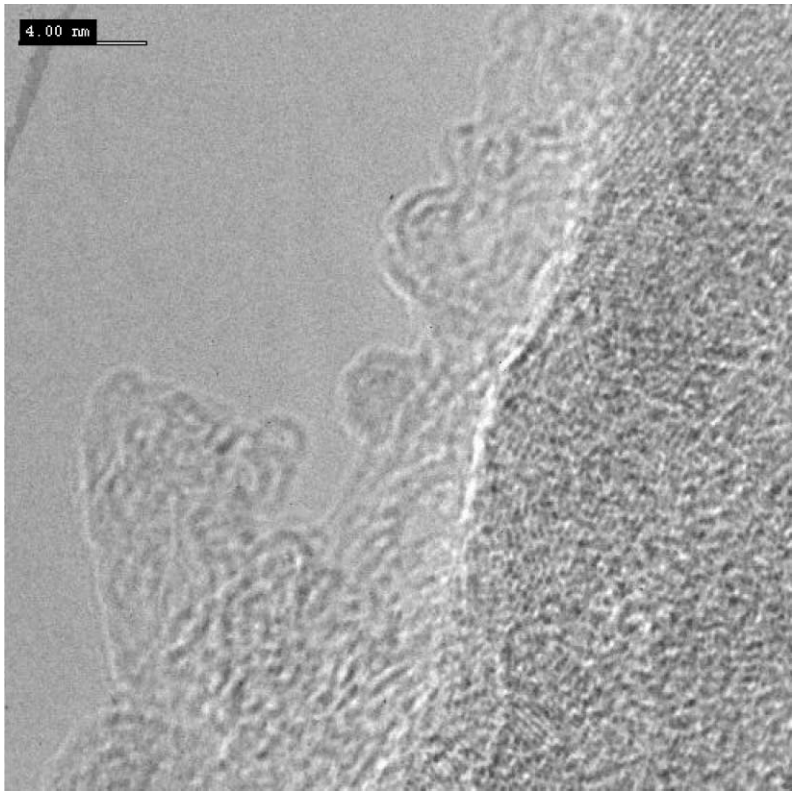

Fig. 4. HRTEM image of a coated $LiMn_2O_4$ particle surface (3 wt.% $LiCoO_2$).

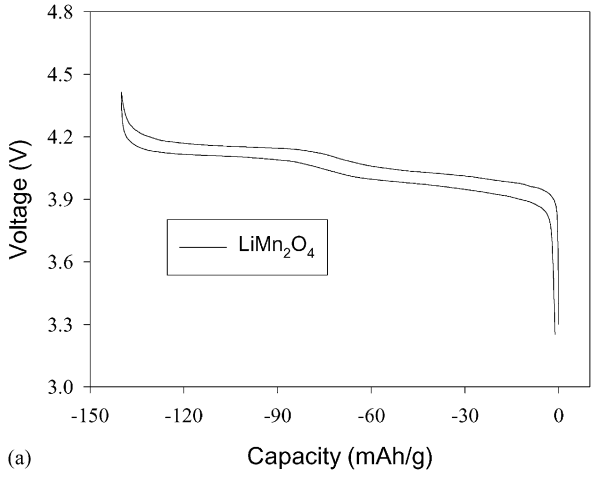

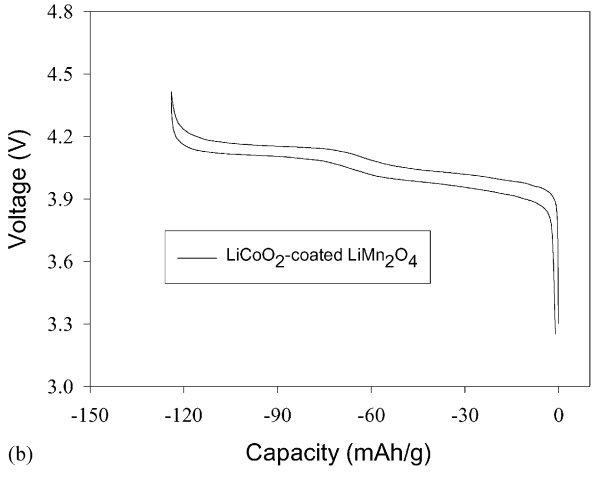

Fig. 5. Typical room temperature charge and discharge curves (at 0.2 mA cm^{-2}) of $LiMn_2O_4$ powder before (a) and after treatment of 5 wt.% $LiCoO_2$ (b) at 25 °C.

to pristine spinel, particularly at a 5 wt.% $LiCoO_2$ concentration. The BET surface area follows a similar general trend, amidst more scattering of the data due to the low measurement values. The decrease in capacity is likely due

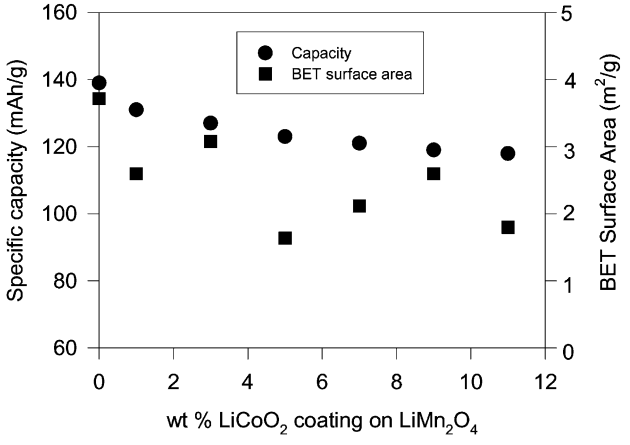

Fig. 6. Third cycle discharge capacity and BET surface of $LiCoO_2$/$LiMn_2O_4$ composites as a function of $LiCoO_2$ content.

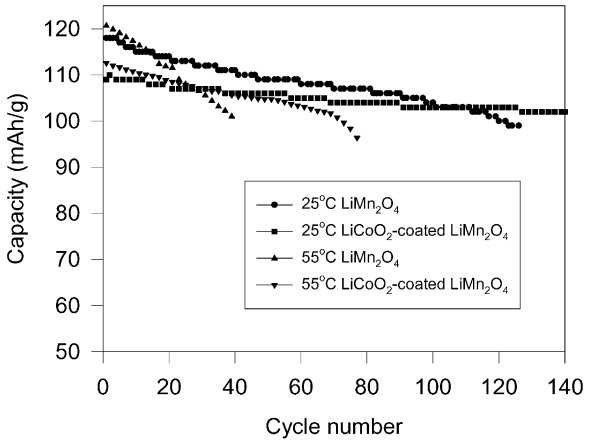

Fig. 7. Cycleability of a Li/$LiMn_2O_4$-coated by 5 wt.% $LiCoO_2$ coin cell at 25 and 55 °C (3.3–4.4 V, 0.5 mA cm^{-2}).

to the difficulty in Li^+ diffusion in the presence of a barrier coating. The $LiCoO_2$ layer also had no apparent Li^+ storage capability. The poor Li^+ conductivity and storage capacity may be traced to the low temperature used in the $LiCoO_2$ synthesis at which the layered structure of $LiCoO_2$ cannot be fully established.

The cycleability of the spinels was tested at two temperatures (25 and 55 °C), using a voltage window of 3.3–4.4 V and a current density of 0.5 mA cm^{-2}. The resulting data are plotted in Fig. 7. At room temperature, the capacity fading over 100 cycles is 12% for pristine $LiMn_2O_4$, but only 5% for $LiCoO_2$-coated $LiMn_2O_4$. Capacity fading is accelerated at the higher temperature of 55 °C, as typical of this family of materials, with the pristine spinel losing about 16% of the initial discharge capacity (120.7 mAh g^{-1}) in 40 cycles. The 5 wt.% $LiCoO_2$-coated $LiMn_2O_4$ fared much better; it loses about 6% of its initial discharge capacity (113 mAh g^{-1}) during the same number of cycles. The $LiCoO_2$ treatment has evidently improved the high-temperature performance of the spinel.

The cause of capacity fade upon repeated charge–discharge cycling has been attributed to a number of factors [22], namely: (i) electrochemical reactions of electrolyte on the charged electrode; (ii) a slow dissolution of spinels according to the disproportionate reaction: $2Mn^{3+} \rightarrow Mn^{4+} + Mn^{2+}$; (iii) a structural transformation due to Jahn–Teller distortion at the discharged state. Jang et al. [1] did not consider the Jahn–Teller distortion to be a major cause of capacity fading in 4 V Li/$LiMn_2O_4$ cells. Rather, they attributed the capacity loss to Mn dissolution which results in two adversarial effects: (i) a material loss of the active component (spinel oxides) and an increase in polarization which results from an increase in cell resistance. When the carbon content in the cathode is low, Mn dissolution is less severe, but this critically affects the contact areas between oxide and carbon particles and leads to a large increase in contact resistance and electrode reaction resistance. Hence, Ohmic polarization would be the dominant factor for the capacity losses in this cathode. For cathodes

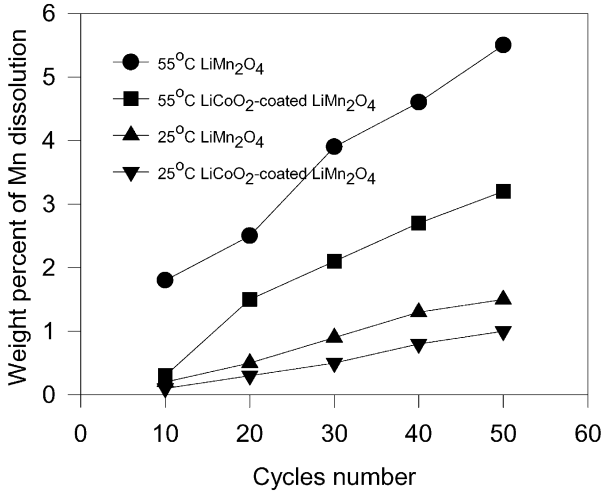

Fig. 8. Mn dissolution in a Li/5 wt.% $LiCoO_2$-coated $LiMn_2O_4$ coin cell as a function of the cycle number. The cell was cycled at 0.5 mA cm^{-2} between 3.3 and 4.4 V at 55 °C.

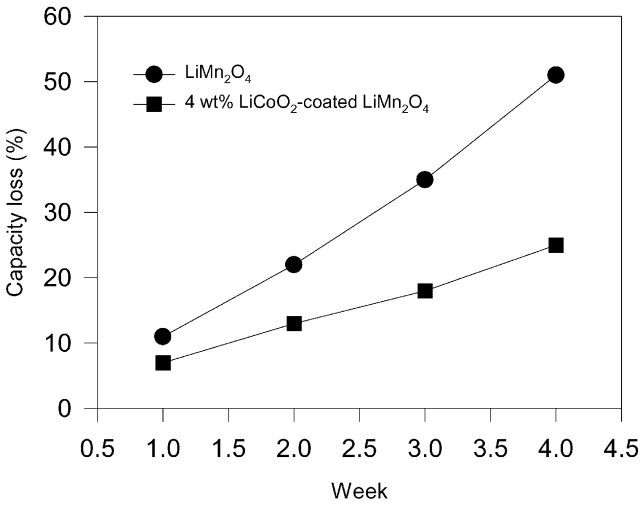

Fig. 9. Self-discharge of fully charged Li-ion cells over a 4-week period.

with an adequate amount of carbon, the Ohmic polarization is less severe, and Mn dissolution accounts for most of the capacity loss. Yoshio and coworkers [23] pointed out the two-phase structure of charged $LiMn_2O_4$ is very sensitive to temperature. The transformation of the unstable two-phase structure to a more stable one-phase structure occurs via the loss of MnO ($Mn^{3+} \rightarrow Mn^{4+} + MnO$), and dominates the capacity fading in cells cycled at room temperature. This process also prevails during cycling at high temperature, together with the direct dissolution of Mn_2O_3. The dissolved Mn^{2+} content is plotted against cycle number in Fig. 8. Dissolution of Mn is definitely more severe at 55 °C. Coating with $LiCoO_2$ has abated the tendency for Mn dissolution, but in the present study, it is unable to eradicate completely the dissolution. The protective value of the $LiCoO_2$ coating comes from the stability of lithium cobalt oxide in the electrolyte. As the $LiCoO_2$ is administered as a barrier coating, it unavoidably increases Li^+ diffusional resistance, and reduces the rate capability of the spinel slightly. The improvement in cycleability at the expense of a slight reduction in capacity is deemed to be a small price to pay.

The self-discharge rates of the spinel electrodes in the fully charged state at 55 °C were determined using the lithium-ion configuration: $LiMn_2O_4$/liquid electrolyte/graphite. $LiMn_2O_4$ coated with 4 wt.% $LiCoO_2$ is effective in reducing the rate of self-discharge. A pristine $LiMn_2O_4$ spinel loses about 50% of its stored capacity after 4 weeks of storage (Fig. 9). A 4 wt.% $LiCoO_2$ coating reduced the capacity loss from 51 to 25%, a very notable improvement. Although these results invariably show that $LiMn_2O_4$ coated with an outer layer of $LiCoO_2$ is effective in reducing the self-discharge rate in the fully-charge state at 55 °C, the mechanism of improvement can only be elucidated after a more thorough characterization of the electrode is completed. Phenomenologically, the coating has prevented direct contact between the spinel and the electrolyte, and suppresses Mn dissolution which is the principal cause of the problem of capacity loss. In this way, the $LiCoO_2$ layer functions primarily as a barrier coating.

4. Conclusions

$LiMn_2O_4$ spinel was coated with lithiated Co oxide using a micro-emulsion process. SEM–EDAX and HRTEM studies have confirmed the presence of a $LiCoO_2$ layer on the $LiMn_2O_4$ core. As $LiCoO_2$ is more stable in the electrolyte than $LiMn_2O_4$, the $LiCoO_2$ coating prevented the direct contact between $LiMn_2O_4$ particles and electrolyte, and hence lessened the possibility of spinel dissolution that is the major cause of capacity loss. The surface treatment is found to be effective in reducing the rate of self-discharge of the spinel, and in improving the cycleability of the spinel, particularly at the elevated temperature of 55 °C. A small decrease in spinel capacity is also noted as the $LiCoO_2$ coating has no apparent Li ion storage capability, and hence functioned primarily as a barrier coating.

Acknowledgements

The authors would like to express their thanks to Mrs. Doreen Lai and Ms. Shue Yin Chow for their experimental assistance.

References

[1] D.H. Jang, Y.J. Shin, S.M. Oh, J. Electrochem. Soc. 143 (1996) 2204.
[2] D. Guyomard, J.M. Tarascon, J. Power Sources 54 (1995) 92.
[3] J.M. Tarascon, F. Coowar, G. Amatucci, F.K. Shokoohi, D. Guyomard, J. Power Sources 54 (1995) 103.

[4] Y. Xia, M. Yoshio, J. Power Sources 66 (1997) 129–133.
[5] D. Guyomard, J.M. Tarascon, J. Electrochem. Soc. 140 (1993) 3071.
[6] G.G. Amatucci, A. Blyr, C. Sigala, P. Alfonse, J.M. Tarascon, Solid State Ionics 104 (1997) 13.
[7] B.K. Palu, S.P. Moulike, J. Dispers. Sci. Technol. 18 (1997) 301.
[8] M. Boutonnet, J. Kizling, P. Stenius, G. Maire, Colloids Surf. 5 (1982) 209.
[9] A. Claerbout, J.B. Nagy, Stud. Surf. Sci. Catal. 63 (1991) 705.
[10] P. Stenius, J. Kizling, M. Boutonnet, U.S. Patent 4425 (1984), p. 261.
[11] K. Kurihara, J. Kizung, P. Stenius, J.H. Fendler, J. Am. Chem. Soc. 105 (1983) 2574.
[12] M. Gobe, K. Kon-no, A. Kitahara, J. Colloid Interface Sci. 93 (1983) 293.
[13] K. Kandori, K. Kon-no, A. Kitahara, J. Colloid Interface Sci. 115 (1987) 579.
[14] K. Kandori, K. Kon-no, A. Kitahara, J. Colloid Interface Sci. 112 (1) (1988) 78.
[15] P. Lianos, K. Thomas, J. Chem. Phys. Lett. 125 (1986) 299.
[16] C.H. Chew, L.M. Gan, D.O. Shah, J. Dispers. Sci. Technol. 11 (1990) 593.
[17] L.M. Gan, B. Liu, C.H. Chew, S.J. Xu, S.J. Chua, G.L. Loy, G.Q. Xu, Langmuir 13 (1997) 6427–6431.
[18] K. Zhang, C.H. Chew, S. Kawi, J. Wang, L.M. Gan, Catal. Lett. 64 (2000) 179–184.
[19] L.M. Gan, H.S.O. Chan, L.H. Zhang, C.H. Chew, B.H. Loo, J. Mater. Chem. Phys. 37 (3) (1994) 263.
[20] L.M. Gan, L.H. Zhang, H.S.O. Chan, C.H. Chew, B.H. Loo, J. Mater. Sci. 31 (1996) 1071.
[21] J.N. Reimers, J.R. Dahn, J. Electrochem. Soc. 139 (1992) 209.
[22] R.J. Gummow, A. de Kock, M.M. Thackeray, Solid State Ionics 69 (1994) 59.
[23] Y. Xia, Y. Zhou, M. Yoshio, J. Electrochem. Soc. 144 (1997) 2593.